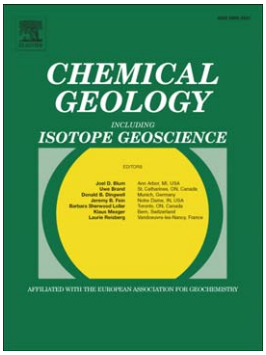

Spatial variability of African dust in soils in a montane tropical landscape in Puerto Rico

M.A. McClintock, G. Brocard, J. Willenbring, C. Tamayo, S. Porder, J.C. Pett-Ridge

PII: S0009-2541(15)00342-3
DOI: doi: 10.1016/j.chemgeo.2015.06.032
Reference: CHEMGE 17650

To appear in: *Chemical Geology*

Received date: 1 March 2015
Revised date: 14 June 2015
Accepted date: 15 June 2015

Please cite this article as: McClintock, M.A., Brocard, G., Willenbring, J., Tamayo, C., Porder, S., Pett-Ridge, J.C., Spatial variability of African dust in soils in a montane tropical landscape in Puerto Rico, *Chemical Geology* (2015), doi: 10.1016/j.chemgeo.2015.06.032

Spatial variability of African dust in soils in a montane tropical landscape in Puerto Rico

M.A. McClintock[1], G. Brocard[2], J. Willenbring[2], C. Tamayo[3], S. Porder[3], and J.C. Pett-Ridge[1]

[1]Department of Crop and Soil Science, Oregon State University, Corvallis, OR, USA.

[2]Department of Earth and Environmental Science, University of Pennsylvania, Philadelphia, PA, USA.

[3]Department of Ecology and Evolutionary Biology, Brown University, Providence, RI, USA.

Corresponding author: J.C. Pett-Ridge, Julie.pett-ridge@oregonstate.edu

Highlights

- Surface soil ε_{Nd} reflects high spatial variability in current African dust content in the Luquillo Mountains, Puerto Rico.
- Soil dust content is more variable than ^{10}Be-based soil denudation rates, implying that both dust retention and dust deposition fluxes are highly spatially variable.
- Soil dust content is positively correlated with biologically cycled phosphorus pools.
- Soil dust content is higher in volcaniclastic-derived soils than in quartz diorite-derived soils.

Abstract

Dust deposition provides rock-derived nutrients such as phosphorus (P) to terrestrial ecosystems. Over pedogenic timescales, as bedrock sources of P are depleted, dust sources of P may support productivity in certain ecosystems, but controls on the spatial variability of dust in montane forested systems are largely unknown. Here, we use neodymium (Nd) isotope ratios in 31 ridgetop surface soils to evaluate the spatial variability of dust contributions to soil across ~100 km^2 in the Luquillo Mountains, Puerto Rico. Dust from the Sahara-Sahel region of Africa carries a distinct isotopic signature of -12 ε_{Nd}. Local bedrock, in contrast, has a ε_{Nd} value of ~+7. End-member mixing calculations based on ε_{Nd} reveal a wide range in dust influence on surface soils, with between 0% and 92% of the top 20 cm of ridgetop soil Nd derived from African dust. Using ε_{Nd} paired with both dust and soil Nd content, the current soil dust content was calculated, ranging from 0 to 8%. There were no correlations between current dust content of soil and ^{10}Be-based denudation rate, elevation, rainfall, longitude, or forest type. Current soil dust content in the Luquillo Mountains is significantly higher in soils developed on volcaniclastic sandstone,

breccia and mudstone than in soils developed on quartz diorite bedrock, which we attribute to greater retention capacity in the volcaniclastic soils. Current soil dust content also increases with increasing ridge-width, implying that small-scale topographic effects and other factors such as wind speed and turbulence influence local dust deposition rates. Higher current dust content of soil is also positively correlated with biologically cycled fractions of soil P on quartz diorite bedrock (r^2=0.24 and p=0.002 for sum of extractable $NaHCO_3$-P + NaOH-P), suggesting that atmospheric dust inputs contribute to the fertility of Luquillo Mountain ecosystems on the relatively P-poor quartz diorite bedrock.

Keywords: atmospheric deposition, Nd isotopes, soil, Luquillo Mountains, African dust, phosphorus, beryllium-10

1. Introduction

Dust emissions from desert areas total as much as 2 billion tons yr^{-1} globally, with multiple important implications for Earth surface processes (Jickells et al., 2005). The global dust cycle affects the radiation budget of the Earth (Tegen et al., 1996), the productivity of ocean-dwelling photosynthetic life (Coale et al., 1996; Martin, 1990), and long-range vectors of bacterial and fungal movement (Shinn et al., 2000). Dust also plays an important role in nutrient cycling and pedogenesis in certain terrestrial ecosystems (e.g. Chadwick et al., 1999; Muhs et al., 2007; Shafer et al., 2007; Soderberg and Compton, 2007).

Ecosystems with highly weathered soils are predicted to experience limiting availability of the rock-derived nutrient phosphorus (P) due to leaching losses and occlusion with iron and aluminum oxides (Walker and Syers, 1976). Even with efficient nutrient recycling, over long timescales small losses of rock-derived P from soil must be replenished by new inputs, such as atmospheric dust deposition or erosion-induced rejuvenation of soil primary minerals from underlying parent material, in order to maintain ecosystem productivity (Chadwick et al., 1999; Pett-Ridge, 2009; Porder et al., 2005). It has been proposed that African dust is an ecologically significant supplier of limiting nutrients to highly productive Amazon Basin ecosystems (Okin et al., 2004; Swap et al., 1992). In this manner, the size of major carbon pools may be linked to factors affecting dust production, transport, and deposition that occur across great distances. At present, however, the number of terrestrial dust records is limited, and even fewer records exist that can be used to examine the spatial variability of dust at a landscape spatial scale or to examine dust inputs over pedogenic timescales of hundreds to thousands of years (Kohfeld and Harrison, 2001; Lawrence and Neff, 2009). Some studies have examined controls on spatial variability of dust in arid regions that are proximal to dust source areas, finding decreasing

windward-leeward soil dust content (Hirmas and Graham, 2011; Pelletier and Cook, 2005; Reheis et al., 1995). Less work has been done on the controls on spatial variability of dust in wetter climates where P depleted soils are more likely to occur, with the exception of Hawaii, where spatial variability of dust inputs appears to be tightly linked to rainfall amount (Porder et al., 2007).

Short-term dust inputs, over the timescale of years, can be estimated directly and indirectly using different techniques, such as measuring non-sea-salt calcium in rainwater (e.g. Stallard, 2001), collecting atmospheric samples pumped through an active filter (e.g. Prospero and Lamb, 2003), or using ocean-basin scale modeling techniques (e.g. Ginoux et al., 2001; Mahowald et al., 2008). These methods are limited by multiple issues, including the high spatial and temporal variability in both transport and deposition (Prospero, 1999). Direct collection of dust using ground-based deposition collectors cannot meaningfully measure the long-term average dust deposition in forested ecosystems, in part because they do not mimic the forest canopy structure and surface properties of leaves (Hicks et al., 1980; Lindberg and Lovett, 1985; Stoorvogel et al., 1997; White and Turner, 1970). Modern deposition studies typically rely on only a few years of data and are thus subject to timescale biases (Pelletier, 2007). Longer timescale data are needed to understand how dust affects soils and nutrient cycling in terrestrial ecosystems, and to understand how variations in climate affect dust inputs to ecosystems.

Isotopic tracers in soils can be used to identify the presence of long-range transported dust (Borg and Banner, 1996; Chabaux et al., 2013; Chadwick et al., 1999; Dia et al., 2006; Kurtz et al., 2001; Li et al., 2013; Pelt et al., 2013; Pett-Ridge et al., 2009b; Viers and Wasserburg, 2004), and to calculate long-term average rates of dust deposition (Pett-Ridge et al., 2009b). Two different isotope systems, strontium ($^{87}Sr/^{86}Sr$) and neodymium ($^{143}Nd/^{144}Nd$) are

commonly used to determine dust provenance (e.g. Kumar et al., 2014). When the dust source region has a unique isotopic signature relative to the deposition region's bedrock, mixing model calculations can be used to calculate the proportion of dust-derived material in a mixture such as soil. This approach works best in situations where dust and underlying bedrock are the only two end-members. This is more often the case with Nd isotopes as compared to Sr isotopes, because sea-salt derived aerosols are presumed to have negligible Nd content (Grousset and Biscaye, 2005).

The Luquillo Mountains of Puerto Rico are well suited for studying dust deposition because there is one dominant dust source region, the Sahara-Sahel region of Africa, and no other significant landmasses in the pathway of dust transport. The predominant wind direction is northeasterly trade winds from the Atlantic Ocean, minimizing the possibility of local or anthropogenic influence on atmospheric inputs. Bedrock formations throughout the Luquillo Mountians have a Nd isotope ratio, expressed as ε_{Nd} , of approximately +7 (Frost et al., 1998; Jolly et al., 1998). The primary dust source in the Luquillo Mountains is the Sahara-Sahel region, which has a very distinct ε_{Nd} value of approximately -12 (Borg and Banner, 1996; Kumar et al., 2014). This creates the opportunity to calculate the fraction of Nd in soil that came from dust. Neodymium isotopes are not believed to be fractionated by weathering processes or biological cycling, and given the age of the Luquillo bedrock relative to the long half life of ^{147}Sm decay to ^{143}Nd (1.06×10^{11} yr^{-1}), incongruent weathering of minerals in Luquillo bedrock is not expected to affect bulk soil $^{143}Nd/^{144}Nd$ ratios (Elderfield et al., 1981; Grousset and Biscaye, 2005). Therefore Luquillo soil Nd isotope ratios should reflect simple mixing between dust and the underlying bedrock.

The goal of this study is to examine the spatial variability of soil dust content in the Luquillo Mountains, and to assess the importance of several likely controls on spatial variability, including topographic, pedogenic, and biotic factors. We present Nd isotopic end-member mixing calculations of current dust content of surface soils spanning a coupled elevation and precipitation gradient, two major bedrock types, and two different forest types across a ~100 km^2 area. Specifically, we test the hypothesis that soil dust content is controlled by orographically-driven precipitation or by forest structure. We also examine the relationship between current soil dust content and surface soil residence times using denudation rates based on cosmogenic nuclides. This comparison allows us to assess the relative importance of variation in soil residence time versus variation in dust deposition rates in controlling the variability in current soil dust content. Finally, we examine the role of dust in supplying P to Luquillo ecosystems.

2. Methods

2.1. Study Site

The Luquillo Mountains are located in the El Yunque National Forest of NE Puerto Rico in the Caribbean and are covered by lower montane, montane, and dwarf rainforest. The climate in El Yunque is classified as tropical, with 2.5 to 5 meters of orographically driven rainfall with little seasonality throughout the year and a mean annual temperature ranging between 24°C at 370 m elevation and 19°C at 1000 m elevation. Trade winds that carry mineral aerosol dust typically travel in a NEE to SWW direction and originate from the Sahara-Sahel region of Africa (Gioda et al., 2013; McClintock et al., in press). The Luquillo Mountains are a Critical Zone Observatory in addition to a Long-Term Ecological Research site, and have been the focus of extensive previous ecology, biogeochemistry, and soil chemistry research. Underlying the study

area, which spans ~100 km^2, there are two different types of bedrock, which correspond to two different primary classifications of soil. Cretaceous andesitic to basaltic volcaniclastic sandstone, breccia, and mudstone bedrock is overlain by Humic Hapludoxes, while Eocene-age intrusive quartz diorite bedrock is overlain by Aquic Dystrudepts (Frost et al., 1998; Jolly et al., 1998; USDA, 2002). Two common forest types covering the sample sites are classified as being dominated by either palo colorado trees with an average canopy height of 15 m, or tabonuco trees with an average canopy height of 20 m (Brokaw et al., 2012). The sites sampled in this study span an elevation range between 376 and 815 meters above sea level (Table 1).

2.2. Sample Collection

Ridgetop soils were collected from a total of 31 locations across the Luquillo Mountains (Table 1). Soils from a fully-factorial investigation of rock type and forest type covering both quartz diorite and volcaniclastic bedrock, and tabonuco and palo colorado forest, were collected from 16 ridgetop locations (4 of each combination) in the summer of 2010 (Mage and Porder, 2013). A second sampling campaign collected soils from an additional 15 sites, all on quartz diorite bedrock with palo colorado forest type. The second set of sites was chosen to constitute a gradient of ridgetop-width, between 2 and 54 m, holding other soil-forming factors constant. Ridge-top sites were defined as having <10% slope, and being local topographic high areas where colluvial deposition of soil from a higher topographical location was unlikely. At each site, 0-20 cm depth soil was collected from three to five sites along the spine of the ridge. The soil samples excluded large roots and the surface litter layer. Soils were air-dried and sieved (<2 mm) within 2 weeks of collection. Samples at each site were composited prior to our analysis. In the initial set of 16 ridgetop soils, a 25 cm by 25 cm quantitative pit was dug to a depth of 20 cm

at each site to determine bulk density. For the 15 ridge-width gradient soils, bulk density was not directly measured and we instead assume a bulk density of 0.75 g cm^{-3} in the top 20 cm, based on the mean of the full range of measured bulk density of 0.61-0.88 g cm^{-3} for similar ridgetop palo colorado quartz diorite soils. Bedrock samples of the Rio Blanco quartz diorite were taken from roadcut locations in the Rio Icacos watershed.

2.3. Sample Analysis

Soils were ashed at 550 °C for five hours, after which approximately 0.4 grams of soil was digested in a microwave using 6 ml HNO_3, 2 ml HCl, and 2 ml HF for 70 minutes (200 °C and 6 MPa). After digestion, samples were dried down on a hotplate, then re-dissolved in a combination of concentrated HCl and HNO_3 and dried down again before a final re-dissolution in weak HNO_3 prior to dilution and analysis.

Rare earth element (REE) and trace element concentrations were analyzed on a Thermo Scientific X-Series II Quadrupole ICP-MS in the William P. Keck Lab for Plasma Spectrometry at Oregon State University. External calibration was done using multi-element standards, and additional single element standards were analyzed to monitor and correct for oxide interferences. An internal indium standard was used to monitor and correct for changes in uptake and instrument sensitivity. Procedural blanks were at similar levels to the instrumental blanks for all trace and REE analytes, <5 pg g^{-1}. Analytical uncertainty of concentration data is 5% based on agreement with published values for trace and REE element concentrations on multiple digestions (n=10) of the NIST 2709a soil standard. Separate subsamples were digested by lithium metaborate flux fusion, and major elements were analyzed on those subsamples by XRF by ALS Chemex (Sparks, NV).

Approximately 60 ng of Sr was purified from each sample using two column chemistry steps. The first step used 1.8 mL Dowex AG50W-X8 (H^+ form) cation exchange resin. The sample was loaded in 1 M HCl, and Sr was eluted with 2M HNO_3. The second step used 50 µL of Eichrom Sr-SPEC ™ resin, where Sr was loaded in 3M HNO_3 and eluted in ultrapure H_2O.

Isotopic measurements were made on a Nu Plasma© multi-collector ICP-MS in the Keck lab at Oregon State University. Masses 83-88 were monitored in static collection mode. Masses 83 and 85 were monitored for Kr (blank only) and Rb (standards and samples) interferences, respectively. Sr isotope ratios were measured 40 times per sample and have internal analytical uncertainties < 0.000020. Reported values are corrected to $^{86}Sr/^{88}Sr = 0.1194$ and Sr standard NBS-987 $^{87}Sr/^{86}Sr = 0.710245$. This instrument measures an average value of 0.70818 and a $2\sigma = 0.000045$ for in house standard EMD (n=205) over the months that our samples were run; this external reproducibility is the experimental precision reported for our Sr-isotope data.

Approximately 150 ng of Nd was isolated from the remainder of the soil sample using a two-stage column procedure. The first step was coincident with the 1.8 mL AG50-X8 resin column used for Sr, and rare earth elements (REE) including Nd were eluted subsequent to the Sr fraction in 6M HNO_3. The REE fraction was converted to 0.1 M HCl and then run through 2 mL of Eichrom Ln-spec™ resin to separate Nd from other REEs; Nd was eluted in 0.25 M HCl. The procedural blank for Nd was <5 pg g^{-1}. The final solutions were all brought to 50 ng g^{-1}concentration and analyzed on the multi-collector ICP-MS in the Keck lab at Oregon State University. The isotopic ratio of Nd is reported in units of ε_{Nd}, using equation 1, where CHUR is the chondritic uniform reservoir of the Earth, with $^{143}Nd/^{144}Nd$ of 0.512638 (Jacobsen and Wasserburg, 1980).

$$\text{Eq. 1} \quad \varepsilon_{Nd} = \left[\frac{\left(\frac{^{143}Nd}{^{144}Nd}\right)_{sample}}{\left(\frac{^{143}Nd}{^{144}Nd}\right)_{CHUR}} - 1 \right] * 10000$$

Long-term precision on this instrument based on 155 analyses of an in-house standard during the period of this study is 0.511205 +/- 0.000014 $^{143}Nd/^{144}Nd$. This corresponds to an analytical precision of 0.3 ε_{Nd}, which is the value used for uncertainty analysis of the data presented here. Analyses of JNdi-1, used for instrumental offset correction, gave similar long-term external reproducibility (0.2 ε_{Nd}; n = 174).

2.4. Phosphorus analyses

Phosphorus fractions were analyzed using a modified Hedley fractionation, extracting sequentially with 0.5N $NaHCO_3$ and 0.1N NaOH (Mage and Porder, 2013; Tiessen and Moir, 1993). Phosphorus data for the "SM" samples in the data tables were previously analyzed as part of a larger dataset in Mage and Porder (2013), while the "PRCT" samples are newly reported here. Each extract was measured for inorganic P on a Westco Smartchem 200 analyzer at Brown University. Each extract was also digested with persulfate and reanalzyed for total P, and organic P was determined by the difference between P in the persulfate digest and P in the undigested extractant. Primary mineral P was also extracted with 1M HCl, but this was less than 5% of total P at all sites and results are not reported here. Every 10th sample was run in triplicate to ensure reproducibility.

2.5. ^{10}Be analyses

We collected selected quartz diorite-derived soil samples for measurement of in situ-produced cosmogenic ^{10}Be in quartz. (The volcaniclastic soils have insufficient quartz for ^{10}Be-based denudation rate analyses). Cosmogenic ^{10}Be is produced by cosmic rays in quartz crystal lattices within the upper few meters of the Earth's surface. The residence time of a quartz grain in the sub-surface depends on the rate at which the overlying material is removed. At steady state, production of ^{10}Be in the soil equals the ^{10}Be lost by erosion at the soil surface, such that ^{10}Be concentration becomes proportional to the denudation rate (Brown et al., 1995; Granger et al., 1996; Lal, 1991). The collected soil samples were processed at the University of Pennsylvania Cosmogenic Isotope Laboratory. Soils were sieved to process the 250-500 µm grain size fraction. Quartz grains were isolated, purified, and dissolved following an adaptation of the protocol in Kohl and Nishiizumi (1992). During final quartz dissolution 250 µg of a carrier characterized by a ^{10}Be/^{9}Be ratio of 1.5 10^{-15} was added to each sample (Scharlau BE03450100 carrier batch 2Q2P – 14/10/10). Beryllium was extracted by ion-exchange chromatography and precipitated as beryllium hydroxide at pH 8-9. Be hydroxide was then oxidized to BeO over an open butane-propane flame, and mixed with Nb powder prior to measurement of the ^{10}Be/^{9}Be ratio by accelerated mass spectroscopy at PRIME lab, Purdue University. Results were normalized to standard 07KNSTD (Nishiizumi et al., 2007) which has a ^{10}Be/^{9}Be ratio of 2.79 x 10^{-11} (Balco, 2009). Procedural blanks yielded ^{10}Be/^{9}Be ratios of 3.5 to 6.0 ± 0.6.10^{-15}. Reported one-sigma uncertainties encompass uncertainties on Purdue AMS measurement, uncertainty on the primary standard, and uncertainties on the blank correction.

2.6 Denudation rate calculations

Production of ^{10}Be at the Earth's surface is affected by spatiotemporal variations in atmospheric pressure and Earth's magnetic field. ^{10}Be-derived soil denudation rates are integrated over the time required to erode 160 g cm^{-2} of soil. The soil denudation rates measured here and in Brown et al. (1995) imply a corresponding integration time ranging between 20 and 50 ka. At this timescale, production rate is expected to vary with the atmospheric changes induced by the glacial cycles. It has been shown however that sea-level lowering by as much as 125 m during the last glaciation had little effect on the atmospheric pressure and cosmic-ray attenuation (Staiger et al., 2007). Redistribution of atmospheric pressure around ice sheets locally had more substantial effects (Staiger et al., 2007), but simulations suggest that in Puerto Rico the maximal effect was less than 2% during the last glacial maximum. Variations in the Earth's magnetic field resulted in time-integrated increase of 0% to 8% of the ^{10}Be production rate with respect to its modern value (Masarik et al., 2001) depending on the latitude. This effect is taken into account by the CHRONUS online calculator ((Balco et al., 2008), version 2.2, 2009, with standardizations values of 2011) used to compute our production rates (Table A1).

Field-specific corrections include the topographic and vegetation shielding. Topographic shielding was calculated following the method of Codilean (2006) using the 1 meter resolution LIDAR DEM of the Luquillo forest, smoothed at 5 meters to remove topographic artifacts. Because samples were taken on interfluves, topographic shielding is minimal and much less than 1%. As a result, total shielding (Table A1) is dominated by vegetation shielding. Vegetation shielding was calculated using the dry biomass values for the palo colorado forest of Zarin and Johnson (1995), adding 20% water to the trunk fraction and 50% water to the leaf fraction (Johnson, pers. com). The resulting shielding (6-7%) is similar to the shielding obtained by Plug et al (2007) in an old-growth temperate rainforest in Washington State. Lateral variations in

cosmic ray attenuation due to vegetation cover patchiness average out with time and are less than 5% after 80 generations of trees (Plug et al., 2007). Palo colorado trees in the Luquillo Mountains have an age distribution dominated by 60 and 200 years modes (Zarin and Johnson, 1995). The long residence time of the quartz in the ^{10}Be production zone therefore amply supports the uniform layer approximation.

For the concentration to be modeled as a total soil denudation rate [D T^{-1}], the mass loss must account for density and be uniform as soil particles are moved through the zone of cosmogenic nuclide production in the upper meters of the soil surface. For soils that undergo extensive weathering, like those in Puerto Rico, the quartz tends to reside in the soil column longer than other minerals. Measuring only quartz leads to a bias toward lower rates because the quartz spends more time in the soil than the average particle. We add a correction for quartz enrichment that varies depending on the location of the soil, thus the quartz enrichment is from 27% on average (Ferrier et al., 2010) up to 91% on ridgetop locations (White et al., 1998). An average vertically integrated wet soil density of 1.6 $g \cdot cm^{-3}$ is used for soil attenuation, based on soil dry densities of 1.2 $g \cdot cm^{-3}$, assuming that soils in the rainforest are close to field capacity year round. Details of denudation rate calculations are provided in the electronic appendix (Tables A1 and A2).

2.7. Dust Calculations

The Nd currently present in soil is a combination of dust-derived Nd and bedrock-derived Nd. Using the soil Nd isotope ratio ε_{Nd}, we can determine the fraction of total soil Nd derived from either dust or rock. The dust endmember has an ε_{Nd} value of -11.8±1.2 s.d., defined based on the average of published values (n=16) for Caribbean aerosols derived from north Africa

(Grousset et al., 1988; Kumar et al., 2014). The Luquillo volcaniclastic bedrock endmember has an average ε_{Nd} of +7.83 ±0.69 (1 s.d.) based on 5 published values (Frost et al., 1998; Jolly et al., 1998), and the quartz diorite end-member has an average ε_{Nd} of +7.19 ±0.62 (1 s.d.) based on 5 published values (Chabaux et al., 2013; Frost et al., 1998; Pett-Ridge et al., 2009b) plus 2 additional samples analyzed here. The fraction of soil Nd that is derived from dust is calculated using a simple two end-member mixing formula (equations 2 and 3), where:

$$\text{Eq. 2} \quad f_{soil-dust}^{Nd} = \left(\frac{\varepsilon_{Nd}^{soil} - \varepsilon_{Nd}^{bedrock}}{\varepsilon_{Nd}^{dust} - \varepsilon_{Nd}^{bedrock}}\right)$$

$$\text{Eq. 3} \quad \%dustNd = 100 f_{soil-dust}^{Nd}$$

For uncertainty analyses, errors were propagated using the 1 s.d. of available dust ε_{Nd} values, and the analytical uncertainty for the soil and bedrock ε_{Nd} values.

The mass of dust-derived Nd (µg cm^{-2}) in the sampled surface 0-20 cm depth range is calculated from the product of the concentration of Nd in soil, and the fraction of Nd that is dust derived. That mass is then divided by the average Nd concentration of Caribbean aerosols derived from north Africa, C^{Nd}_{dust} (43 ug g^{-1}, n=44, 1 s.d. ±7), (Grousset et al., 1988; Grousset et al., 1992; Muhs et al., 1987; Trapp et al., 2010) to determine the current mass of accreted dust in the top 20 cm (g cm^{-2}) (equation 4).

$$\text{Eq. 4} \quad \%Dust = 100\left(\frac{f_{soil-dust}^{Nd} C_{soil}^{Nd}}{C_{dust}^{Nd}}\right)$$

For uncertainty analyses, errors were propagated using the 1 s.d. of available C^{Nd}_{dust} values, and the analytical uncertainty for the C^{Nd}_{soil} values.

Other studies have employed variations on a mass transfer function, or "τ" calculation based on immobile index elements such as Zr or Nb (Brimhall and Dietrich, 1987; Kurtz et al., 2000) specifically to determine soil dust inputs, (e.g. Ferrier et al., 2011; Pett-Ridge, 2007). In the Luquillo Mountains, weathering intensity is high enough that the less mobile index elements are significantly mobilized during chemical weathering. For example, using Zr depth profile data, there is either a ~50% volume dilation during weathering of Luquillo quartz diorite-derived saprolite, which contradicts previous evidence of isovolumetric weathering at that site (White et al., 1998), or, more likely, an ~50% loss of Zr during saprolite weathering (Pett-Ridge, 2007). For this reason, an immobile index element-based calculation of soil dust inputs is not performed here. We do, however, present the results of a tau calculation for Nd in the surface soils for discussion purposes (Table 2). The tau (τ) value quantifies the gain or loss of an element in soil relative to underlying bedrock using equation 5:

$$\text{Eq. 5} \quad \tau_{j,w} = \left[\frac{C_{j,w} C_{Nb,p}}{C_{Nb,w}\, C_{j,p}} - 1\right]$$

where $\tau_{j,w}$ is the relative loss or gain of element *j* from soil with respect to parent material, $C_{j,w}$ is the concentration of element j in soil and $C_{j,p}$ is the concentrations of element *j* in bedrock, $C_{Nb,w}$ and $C_{Nb,p}$ are the concentrations of the index element Nb in soil and bedrock, respectively. We use Nb as an index element based on work showing it is a least mobile element in high rainfall soils (Kurtz et al., 2000). A tau-value of +1 indicates 100% gain relative to bedrock, while a value of -1 indicates complete elemental loss relative to bedrock contribution.

3. Results

3.1. Elemental Analysis

A wide range of surface soil Nd concentrations is evident across the 31 ridgetop sites, from 0.28 to 8.98 μg g^{-1} (Table 2). Based on 15 rock samples collected in the same quartz diorite subwatersheds where soils were sampled, the quartz diorite bedrock has a Nd concentration of 7.95± 0.27 μg g^{-1} (1s.e.). Based on 29 rock samples from across the volcaniclastic subwatersheds where soils were sampled, the volcaniclastic bedrock has an average Nd concentration of 12.91 ± 0.9 μg g^{-1} (1s.e.). The average Nd concentration in soils developed from volcaniclastic bedrock is 3.24 ± 0.47 μg g^{-1} (1s.e.), while the average Nd concentration in soils developed on quartz diorite is 2.34 ± 0.45 μg g^{-1} (1s.e.).

3.2. Nd isotopes

The ε_{Nd} values for all 31 of the 0-20 cm depth ridgetop soils span a wide range, from -10.3 to 7.3 with an average value of –3.6 in volcaniclastic soils and an average of -0.8 in quartz diorite soils (Table 2). The values encompass nearly the entire range between the two end-members (dust has an ε_{Nd} of -11.8, while both bedrock types in Luquillo have a ε_{Nd} of +7.2 and +7.8). Average ε_{Nd} soil values were not statistically significantly different from each other ($p>0.05$) based on underlying bedrock type or based on forest type. Across all soils, ε_{Nd} was not correlated to elevation, rainfall, latitude, or longitude based on single or multivariate linear regression analysis. Using equation 3, the dust-derived Nd across all the soils ranges from 0 to 92%. Figure 1 shows a map of dust-derived Nd. The average dust-derived Nd in soils developed from volcaniclastic bedrock was 58 ± 8% (1s.e.), slightly higher than the average dust-derived Nd in soils developed on quartz diorite of 42 ± 6% (1s.e.).

3.3 Soil dust content

Calculations of the current soil dust content (equation 4) yield a range from 0 to 8% across all ridgetop surface soils (Table 2 and Figure 2). Of the 31 sites studied here, only one site does not show evidence of dust inputs. That one site, PRGB140324-3, occurs below the elevation of a regional topographic knickpoint, which has faster eroding soils below and slower eroding soils above (Brocard et al., 2015), and that site is the only knife-edge ridge in our sampling that occurred below the knickpoint. The mean dust content of soils developed on volcaniclastic bedrock is 3.9 ± 0.6% (1s.e.), which is significantly higher ($p < 0.01$) than the mean dust content of soils developed on granodiorite bedrock, 1.3 ± 0.2% (1s.e.), based on a one-way ANOVA with bedrock type as the factor. Within rock types, there are no significant correlations in soil dust content with forest type, elevation, rainfall, latitude, or longitude, using either single or multivariate regression.

3.4 Soil phosphorus (P)

Soil P data for 0-20 cm depth of 28 ridgetop soils are shown in Table 4. The average total soil P concentration in the volcaniclastic soils was significantly higher than in quartz diorite soils (mean of 219 ± 13.3 μg g^{-1} (1s.e.) versus mean of 166 ± 11.1 μg g^{-1} (1s.e.), respectively). Of the extractable P fractions, NaOH-extractable organic P represented the largest fraction, constituting, on average, 28% of the total P, while NaOH-extractable inorganic P represented an average of 13% of total P. Sodium bicarbonate-extractable P ($NaHCO_3$-P_t) was a small fraction, representing, on average, 2% of total soil P, and was predominately $NaHCO_3$-P_o.

4. Discussion

Incorporation of African dust into Luquillo Mountain ecosystems is widespread based on Nd isotope evidence (Table 2). The percent of dust-derived Nd in surface ridegetop soils exhibits large variation across the landscape, from primarily autochthonous in some places to primarily allochthonous Nd in others (Figure 1). The current dust content of the soil, ranging between 0 and 8% across all soils, likely reflects only a fraction of the total mass of dust accreted over the residence time of the sampled soil depth interval (0-20 cm). Both the dust itself and the dust-derived Nd tracer are unlikely to be well-preserved in the soil, given the intense weathering conditions and the observed bioturbation in Luquillo soils, and due to large mobilization and redistribution of Nd which occurs during chemical weathering (e.g. Nesbitt and Markovics, 1997; Nesbitt and Wilson, 1992).

A variety of lines of evidence (mass fluxes, primary mineral dissolution at depth, quartz and kaolinite dissolution at the surface) suggest chemical weathering in Luquillo soils is rapid and intense (e.g. Ferrier et al., 2010; Schulz and White, 1999; White et al., 1998). Elemental mass transfer calculations (τ_{Nd}, using Nb as an index element) that compare the inventory of Nd in soil to that in the underlying bedrock show losses averaging 90% (Table 2). If the additional inputs due to dust could be taken into account, the true total Nd loss from soils would be even greater. While it is clear that Nd is mobile, uncertainties about the leaching rate of Nd from dust-derived minerals in Luquillo soils prevent the calculation of the total loss rate and dust input flux. However, there is reason to believe the dust-derived Nd may leach faster than rock-derived Nd. A Sr-Nd isotope-isotope mixing plot shows that most surface soils reflect a mixture between atmospheric inputs and underlying saprolite, as opposed to a mixture of atmospheric inputs and underlying rock (Figure 3). Functionally, this means that most dust in the Luquillo Mountains

accretes into an already highly weathered matrix. The mineralogy of the dust is less weathered, consisting predominately of illite, with lesser amounts of montmorillinite, kaolinite, feldspars, gypsum, calcite, and biogenic material (Reid et al., 2003). For this reason, upon incorporation into Luquillo surface soils, dust minerals may be more reactive than autochthonous soil minerals that have already undergone extensive weathering in the saprolite and soil.

Both rock and dust-derived Nd are further susceptible to leaching through iron-(oxy)hydroxide mineral atom exchange and recrystallization processes that occur in Luquillo soils that are known to expel associated trace elements such as Nd (Frierdich and Catalano, 2012; Pedersen et al., 2005; Tishchenko et al., 2015). In addition to chemical mobilization, earthworm bioturbation in Luquillo soils is a physical mechanism that translocates minerals from the surface deeper into soil profiles (Gonzalez et al., 1996). Clear evidence for the the mobilization of dust-derived Nd deeper into Luquillo quartz diorite weathering profiles is found in ε_{Nd} depth profiles, which show the signature of African dust at 2 and 3 m depth (Chabaux et al., 2013; Pett-Ridge et al., 2009b).

4.1. Controls on the spatial variability of current soil dust content

Spatial variability in current soil dust content has many potential controls, including factors that influence dust deposition rate and dust scavenging from the atmosphere, and factors that affect the retention of accreted dust in soil. Correlation analysis of current soil dust content with the environmental variables of latitude, longitude, elevation, or forest type revealed no clear patterns to explain wide spatial variation in soil dust content across ridgetop soils in the Luquillo Mountains. The current soil dust content was significantly different, however, between soils developed on the two bedrock types. Oxisols developed on volcaniclastic bedrock had higher

dust content than inceptisols developed on quartz diorite bedrock (Figure 4). This difference in mean dust content between the two soil types may be controlled by some combination of differences in surface soil residence times or the different mineralogical and chemical environment between the two soil types, and their resulting tendency to retain accreted dust. The Fe content of the volcaniclastic soils is higher, averaging 11.4 ± 0.4% Fe_2O_3 (1s.e.), while the quartz diorite soils average 4.5 ± 0.4% Fe_2O_3 (1s.e.). The Fe content of the volcaniclastic soils is known to occur as highly reactive short-range ordered mineral phases (Tishchenko et al., 2015). Similarly, the Al content of the volcaniclastic soils is higher, averaging 22.5 ± 0.6% Al_2O_3 (1s.e.), while the quartz diorite soils averaged 12.8 ± 0.5% Al_2O_3 (1s.e.). While we did not characterize the specific carrier phases of Nd in surface soils, both Fe-(oxy)hydroxide minerals and hydrous aluminum phosphates are known to incorporate rare earth elements (Braun et al., 1998; Land et al., 1999; Walter et al., 1995), providing a potential mechanism for greater retention of the dust-derived Nd signal in volcaniclastic soils.

Elevation and rainfall are closely linked in the Luquillo Mountains, with higher rainfall at higher elevations due to adiabatic cooling (Daly et al., 2003). Forest structure is also linked to elevation and rainfall, with shorter trees and higher density of shrubs and epiphytes at higher elevations. The cloud condensation level occurs at 600 m altitude; above this elevation soils have higher saturation frequencies and qualify as hydric. Relative humidity and windspeed are also higher at higher elevations. Given these elevational differences, the lack of correlation between current soil dust content and rainfall or elevation (which strongly co-vary), or location with respect to the dominant NEE-SWW airmass trajectories was somewhat surprising. In contrast, in Hawaii, the spatial variation of dust incorporated in soil is clearly positively correlated with the amount of rainfall and with increasing elevation (Porder et al., 2007). The

difference in controls in spatial variability may be caused by the much more complex mountainous topography in the Luquillo Mountains, relative to the more simple case of large shield volcanoes in Hawaii. In addition, the rainfall among the ridgetop sites studied here varied between 3538 and 4552 mm yr^{-1}, a relatively smaller range compared to the climate gradient in Hawaii where soil dust was quantified (~250-3000 mm yr^{-1}). The precipitation range in the Luquillo mountains may be too small to see an effect of orographically-driven rainfall scavenging of dust given other confounding factors. In addition to larger-scale landscape factors, local microclimate variables such as surface wind speed and wind turbulence play an important role in controlling local scale variation in dust deposition (Zhang et al., 2014).

The role of biotic factors in controlling current soil dust content is not apparent in our data. Elsewhere, surface canopy characteristics have been shown to play an important role in capturing dust. For example, differences in leaf morphology and surface area of conifers relative to broadleaf trees strongly influence the amount of dust scavenged by the forest canopy (Gosz et al., 1983). In the Yucatan Peninsula of Mexico, Lawrence et al (2007) found that forest stature controls atmospheric inputs, with a mature forest 12 m tall capturing twice as much atmospheric inputs as a 6m tall young forest. In contrast, in the Luquillo Mountains, our data from 7 ridgetop soil sites with tabonuco forest, with a typical canopy height of 20 m, and 24 ridgetop soil sites with palo colorado forest, with a typical canopy height of 15 m, did not have significantly different soil dust content. It is perhaps not surprising given the small sample size and the moderate difference in canopy height that the effect of forest type was not apparent. Furthermore, the historical surface canopy characteristics over the approximately thousand year residence times of the surface 0-20 cm of soil is unknown but likely quite variable. Current spatially-explicit forest canopy structure can be quantified with LIDAR data, but given the rapid

rates of change in forest structure over short timescales, the modern data are not expected to reflect the longer-term (Dubayah et al., 2010; Meyer et al., 2013). Spatial variation in bioturbation is another possible biotic factor controlling current surface soil dust content. In the Luquillo Mountains, earthworm abundance does not vary between palo colorado and tabonuco forest (Gonzalez et al., 1996). However, upland forests and wetter soils have more earthworms. If higher elevation, higher rainfall locations have greater dust deposition inputs, then concurrent higher bioturbation at those sites may reduce the signal of dust in those surface soils.

Variation in denudation rates across the landscape and the resulting variation in soil residence times may also control the imprint of dust in surface soils. Within 16 ridgetop quartz diorite soils with palo colorado forest, ^{10}Be-based denudation rates derived from quartz in soils are moderately variable, ranging between 42 ± 9 and 73 ± 3 mm ka^{-1} (Table 3), and these rates agree well with previous estimates of denudation in the quartz diorite Luquillo landscape (Brown et al., 1995; Pett-Ridge et al., 2009b; Riebe et al., 2003; White et al., 1998). There is no correlation between dust content and denudation rate (Figure 5), however, which means that variation in the length of time available for dust accumulation is not a primary control on soil dust content variation. In addition, there is notably less variation in denudation rate (~2-fold) than the variation in dust content (~11-fold) among these 16 sites. Given that these 16 ridgetop sites are relatively close to each other, have the same soil type, forest type, and span a narrow rainfall range of 3830 mm yr^{-1} to 4150 mm yr^{-1}, we do not expect large variation in leaching and bioturbation rates. We therefore interpret differences in soil dust content to primarily reflect differences in dust deposition rates as opposed to being only driven by differences in denudation rates.

Based on quartz diorite ridegetop sites, soils on wider ridges have higher dust contents (r^2 = 0.66; p = 0.01, Figure 6), although wider ridges do not have lower denudation rates. The lack of a relationship between ridge-width and denudation was unexpected, and implies that other factors control increasing soil dust content with increasing ridge-width. It is not known what causes higher current soil dust content on wider ridges, but in the absence of a residence time effect, it appears that small-scale meteorological factors related to airmass interactions with ridges, or local differences in forest canopy structure may play a role. These factors create high spatial variability, especially in dry deposition (Zhang et al., 2014). Recent work comparing wet-only and bulk precipitation inputs and openfall and throughfall precipitation inputs in the Luquillo Mountains found that despite overall high precipitation rates, dry deposition appears to account for at least 50% of dust inputs (McClintock et al., in press).

4.2. Implications of dust inputs for phosphorus cycling

The spatial variation in soil dust content we observe across a ~100 km^2 montane landscape may reflect a wide variation in atmospheric phosphorous (P) delivery to Luquillo Mountain ecosystems. Previous work in the quartz diorite Rio Icacos watershed within the Luquillo Mountains estimated dust-derived P inputs of between 0.15 to 0.31 kg ha^{-1} yr^{-1}, on the same order of magnitude as the estimated denudation-driven saprolite inputs of P to soil of between 0.07 to 0.19 kg ha^{-1} yr^{-1} (Pett-Ridge, 2009). Phosphorus is likely to limit many important biogeochemical processes in tropical forests (Vitousek et al., 2010), and Luquillo is no exception. Based on fertilization studies of nutrient limitation (Fetcher et al., 1996), and an extensive evaluation of soil nutrient status (Silver et al., 1994), there is evidence that Luquillo ecosystems may be P limited. Availability of soil P is limited by the strong affiliation of P for

the abundant Fe-(oxy)hydroxide minerals in Luquillo soils (Chacon et al., 2006). Phosphorus availability is also limited by deep weathering profiles (at least 8-10 m deep on many ridges), which physically separate the rooting zone from fresh rock-derived P (Buss et al., 2010; White et al., 1998).

Parent material P content is known to be a major driver of soil phosphorus status both globally (Porder and Ramachandran, 2013), and specifically in the Luquillo Mountains, with higher soil P contents in soils developed on the more P-rich volcaniclastic bedrock (Mage and Porder 2013). We analyzed the relationships between both total and extractable soil P content with elevation, rainfall, carbon (C), Fe, Al, and dust content in the ridgetop soils. Dust content within the volcaniclastic-derived soils does not correlate with soil P fractions (n=9). Within quartz-diorite-derived soils (n=19), we find that dust content explains a significant amount of the variability in soil P (Figure 7). Dust explains 25% of the variance in total soil P content, and 24% of the variance in extractable P ($NaHCO_3$ +NaOH). The $NaHCO_3$ and NaOH extractions are thought to represent biologically cycled P pools and P adsorbed on Fe and Al oxides which may become biologically active during intermittent anaerobic conditions in wet tropical forests (Chacon et al., 2006; Johnson et al., 2003; Liptzin and Silver, 2009; Yang and Post, 2011). This is not a large percentage of the variance, but it is larger than that which can be explained by rainfall ($r^2 = 0$, and $r^2 = 0.17$, for total P and extractable P) or elevation ($r^2 = 0.001$, and $r^2 = 0.13$, for total P and extractable P). The $NaHCO_3$ and NaOH-extractable P pools are not correlated with % C in soil, which suggests that the correlation between potentially biologically cycled P and soil dust content is not simply driven by the amount of organic matter in the soil. Further, within the quartz diorite soils, Fe and Al content is not correlated with either extractable or total P. In soils developed on the more P-poor quartz diorite bedrock, dust inputs therefore appear to

play a small but non-negligible role in increasing the amount of biologically cycled P in ecosystems and soils, similar to what has been observed in dust fertilization of ecosystems in Hawaii and Japan (Chadwick et al., 1999; Hartmann et al., 2008; Nakano et al., 2012).

Overall, available data on the solubility of P in African dust suggests that is likely to be greater than that of the P in saprolite that enters Luquillo soils from below. Recent work showed that aerosol phosphorus from North African air masses was 15.5 ±14.1 % soluble in just pure water (Longo et al., 2014). Apatite is abundant in Saharan-Sahel dust, although exchangeable, organic, and Fe-mineral associated P is also present (Eijsink et al., 2000; Herut et al., 2002; Moreno et al., 2006; Singer et al., 2004). Dust from the Saharan Bodélé Depression specifically, which is a major source of the overall North African dust emissions, indicates that biogenic apatite P in the form of fish bone and scales contributes a significant fraction of the total P load (Hudson-Edwards et al., 2014). During weathering of Luquillo bedrock, bedrock P in the form of apatite dissolves completely and rapidly at the saprolite –bedrock interface, and most P in the saprolite is associated with Fe and Al oxides (Buss et al., 2010). Dust-derived P that accretes into surface soils is therefore likely to be more available and more efficiently utilized by the biomass, as has been observed for dust-derived P inputs elsewhere (Eger et al., 2013). Dust accretion can therefore counteract natural ecosystem regression by providing more readily available P and by providing it directly to the surface where the plants roots and microbial P cycling are concentrated. We suggest that understanding the controls on spatial variability in atmospheric dust inputs will therefore contribute to the understanding of soil fertility and ecosystem nutrient cycling in many landscapes.

5. Conclusions

Nd isotopes used to trace African dust inputs and calculate the current soil dust content in 31 ridgetop surface soils across the Luquillo Mountains in Puerto Rico show that dust inputs are widespread and spatially variable. We did not observe an expected decline in soil dust content along windward-leeward airmass trajectories, or an increase in dust content with increasing rainfall. In terms of topographic, climatic, and biotic factors, we saw only a clear influence of ridge width on soil dust content, suggesting that in complex mountainous topography, multiple factors likely play a role in controlling dust inputs to soil, and likely reflecting the importance of dry deposition relative to wet. We also observed a lithological effect, which highlights the role of underlying lithology in controlling the mineralogical and chemical environment of surface soils, which in turn controls the degree and timescale over which geochemical and isotopic tracers are retained in soil during chemical weathering. We suggest that local meteorological variables that relate to dry deposition of dust, such as local wind speed and turbulence, can be used to improve our ability to predict dust inputs across landscapes and in turn assess the potential influence of dust on terrestrial nutrient cycling.

Acknowledgements

Brian Haley is thanked for assistance with the Nu Plasma MC-ICP-MS analyses in the W.M. Keck Collaboratory for Mass Spectrometry at Oregon State University, and for helpful comments on an earlier draft of this manuscript. Noelle Moen and April Abbott are also thanked for assistance with Sr isotope analysis. Support was provided by the Luquillo Critical Zone Observatory, NSF EAR-1331841. JKW and GYB acknowledge NSF grant 1349261.

References

Balco, G., 2009. 26Al-10Be exposure age/erosion rate calculators: update from v. 2.1 to v. 2.2 CRONUS Online Calculator, http://hess.ess.washington.edu.

Balco, G., Stone, J.O., Lifton, N.A., Dunai, T.J., 2008. A complete and easily accessible means of calculating surface exposure ages or erosion rates from (10)Be and (26)Al measurements. Quaternary Geochronology, 3(3): 174-195.

Borg, L.E., Banner, J.L., 1996. Neodymium and strontium isotopic constraints on soil sources in Barbados, West Indies. Geochimica et Cosmochimica Acta, 60(21): 4193-4206.

Braun, J.J., Viers, J., Dupre, B., Polve, M., Ndam, J., Muller, J.P., 1998. Solid/liquid REE fractionation in the lateritic system of Goyoum, east Cameroon: The implication for the present dynamics of the soil covers of the humid tropical regions. Geochimica Et Cosmochimica Acta, 62(2): 273-299.

Brimhall, G.H., Dietrich, W.E., 1987. Constitutive mass balance relations between chemical-composition, volume, density, porosity, and strain in metasomatic hydrochemical systems: Results on weathering and pedogenesis. Geochimica et Cosmochimica Acta, 51(3): 567-587.

Brocard, G., Willenbring, J., Scatena, F., Johnson, A.H., 2015. Effects of a tectonically-triggered wave of incision on Riverine Exports and Soil Mineralogy in the Luquillo Mountains of Puerto Rico. Journal of Applied Geochemistry, in press.

Brokaw, N., Crowl, T., Lugo, A.E., McDowell, W.H., Scatena, F., Waide, R.B., Willig, M., 2012. A Caribbean Forestry Tapestry. Oxford University Press.

Brown, E.T., Stallard, R.F., Larsen, M.C., G.M., R., Yiou, F., 1995. Denudation rates determined from the accumulation of *in situ* produced ^{10}Be in the Luquillo Experimental Forest, Puerto Rico. Earth and Planetary Science Letters, 129: 193-202.

Buss, H.L., Mathur, R., White, A.F., Brantley, S.L., 2010. Phosphorus and iron cycling in deep saprolite, Luquillo Mountains, Puerto Rico. Chemical Geology, 269(1-2): 52-61.

Chabaux, F., Blaes, E., Stille, P., Roupert, R.D., Pelt, E., Dosseto, A., Ma, L., Buss, H.L., Brantley, S.L., 2013. Regolith formation rate from U-series nuclides: Implications from the study of a spheroidal weathering profile in the Rio Icacos watershed (Puerto Rico). Geochimica Et Cosmochimica Acta, 100: 73-95.

Chacon, N., Silver, W.L., Dubinsky, E.A., Cusack, D.F., 2006. Iron reduction and soil phosphorus solubilization in humid tropical forests soils: The roles of labile carbon pools and an electron shuttle compound. Biogeochemistry, 78(1): 67-84.

Chadwick, O.A., Derry, L.A., Vitousek, P.M., Huebert, B.J., Hedin, L.O., 1999. Changing sources of nutrients during four million years of ecosystem development. Nature, 397(6719): 491-497.

Coale, K.H., Johnson, K.S., Fitzwater, S.E., Gordon, R.M., Tanner, S., Chavez, F.P., Ferioli, L., Sakamoto, C., Rogers, P., Millero, F., Steinberg, P., Nightingale, P., Cooper, D., Cochlan, W.P., Landry, M.R., Constantinou, J., Rollwagen, G., Trasvina, A., Kudela, R., 1996. A massive phytoplankton bloom induced by an ecosystem-scale iron fertilization experiment in the equatorial Pacific Ocean. Nature, 383(6600): 495-501.

Codilean, A.T., 2006. Calculation of the cosmogenic nuclide production topographic shielding scaling factor for large areas using DEMs. Earth Surface Processes and Landforms, 31(6): 785-794.

Daly, C., Helmer, E.H., Quinones, M., 2003. Mapping the climate of Puerto Rico, Vieques and Culebra. International Journal of Climatology, 23(11): 1359-1381.

Dia, A., Chauvel, C., Bulourde, M., Gerard, M., 2006. Eolian contribution to soils on Mount Cameroon: Isotopic and trace element records. Chemical Geology, 226(3-4): 232-252.

Dubayah, R.O., Sheldon, S.L., Clark, D.B., Hofton, M.A., Blair, J.B., Hurtt, G.C., Chazdon, R.L., 2010. Estimation of tropical forest height and biomass dynamics using lidar remote sensing at La Selva, Costa Rica. Journal of Geophysical Research-Biogeosciences, 115.

Eger, A., Almond, P.C., Condron, L.M., 2013. Phosphorus fertilization by active dust deposition in a super-humid, temperate environment-Soil phosphorus fractionation and accession processes. Global Biogeochemical Cycles, 27(1): 108-118.

Eijsink, L.M., Krom, M.D., Herut, B., 2000. Speciation and burial flux of phosphorus in the surface sediments of the Eastern Mediterranean. American Journal of Science, 300(6): 483-503.

Elderfield, H., Hawkesworth, C.J., Greaves, M.J., Calvert, S.E., 1981. Rare-earth element geochemistry of oceanic ferromanganese nodules and associated sediments. Geochimica Et Cosmochimica Acta, 45(4): 513-528.

Ferrier, K.L., Kirchner, J.W., Finkel, R.C., 2011. Estimating millennial-scale rates of dust incorporation into eroding hillslope regolith using cosmogenic nuclides and immobile weathering tracers. Journal of Geophysical Research-Earth Surface, 116.

Ferrier, K.L., Kirchner, J.W., Riebe, C.S., Finkel, R.C., 2010. Mineral-specific chemical weathering rates over millennial timescales: Measurements at Rio Icacos, Puerto Rico. Chemical Geology, 277(1-2): 101-114.

Fetcher, N., Haines, B.L., Cordero, R.A., Lodge, D.J., Walker, L.R., Fernandez, D.S., Lawrence, W.T., 1996. Responses of tropical plants to nutrients and light on a landslide in Puerto Rico. Journal of Ecology, 84(3): 331-341.

Frierdich, A.J., Catalano, J.G., 2012. Controls on Fe(II)-Activated Trace Element Release from Goethite and Hematite. Environmental Science & Technology, 46(3): 1519-1526.

Frost, C.D., Schellekens, J., Smith, A., 1998. Nd, Sr, and Pb isotopic characterization of Cretaceous and Paleogene volcanic and plutonic island arc rocks from Puerto Rico. In: Lidiak, E.G.a.L., D. K. (Ed.), Tectonics and Geochemistry of the Northeastern Caribbean. Geological Society of America Special Paper, Boulder, Colorado, pp. 123-132.

Ginoux, P., Chin, M., Tegen, I., Prospero, J.M., Holben, B., Dubovik, O., Lin, S.J., 2001. Sources and distributions of dust aerosols simulated with the GOCART model. Journal of Geophysical Research-Atmospheres, 106(D17): 20255-20273.

Gioda, A., Mayol-Bracero, O.L., Scatena, F.N., Weathers, K.C., Mateus, V.L., McDowell, W.H., 2013. Chemical constituents in clouds and rainwater in the Puerto Rican rainforest: Potential sources and seasonal drivers. Atmospheric Environment, 68: 208-220.

Gonzalez, G., Zou, X.M., Borges, S., 1996. Earthworm abundance and species composition in abandoned tropical croplands: Comparisons of tree plantations and secondary forests. Pedobiologia, 40(5): 385-391.

Gosz, J.R., D. G. Brookins, Moore, D.I., 1983. Using strontium isotope ratios to estimate inputs to ecosystems. BioScience, 33: 23-30.

Granger, D.E., Kirchner, J.W., Finkel, R., 1996. Spatially averaged long-term erosion rates measured from in situ-produced cosmogenic nuclides in alluvial sediment. Journal of Geology, 104(3): 249-257.

Grousset, F.E., Biscaye, P.E., 2005. Tracing dust sources and transport patterns using Sr, Nd and Pb isotopes. Chemical Geology, 222(3-4): 149-167.

Grousset, F.E., Biscaye, P.E., Zindler, A., Prospero, J., Chester, R., 1988. Neodymium isotopes as tracers in marine sediments and aerosols: North Atlantic. Earth and Planetary Science Letters, 87(4): 367-378.

Grousset, F.E., Rognon, P., Coudegaussen, G., Pedemay, P., 1992. Origins of peri-Saharan dust deposits traced by their Nd and Sr isotopic composition. Palaeogeography Palaeoclimatology Palaeoecology, 93(3-4): 203-212.

Hartmann, J., Kunimatsu, T., Levy, J.K., 2008. The impact of Eurasian dust storms and anthropogenic emissions on atmospheric nutrient deposition rates in forested Japanese catchments and adjacent regional seas. Global and Planetary Change, 61(3-4): 117-134.

Herut, B., Collier, R., Krom, M.D., 2002. The role of dust in supplying nitrogen and phosphorus to the Southeast Mediterranean. Limnology and Oceanography, 47(3): 870-878.

Hicks, B.B., Wesely, M.L., Durham, J.L., 1980. In: Critique of methods to measure dry deposition: Workshop summary. U.S. Environmental Sciences Research Laboratory, Research Triangle Park, NC.

Hirmas, D.R., Graham, R.C., 2011. Pedogenesis and Soil-Geomorphic Relationships in an Arid Mountain Range, Mojave Desert, California. Soil Science Society of America Journal, 75(1): 192-206.

Hudson-Edwards, K.A., Bristow, C.S., Cibin, G., Mason, G., Peacock, C.L., 2014. Solid-phase phosphorus speciation in Saharan Bodélé Depression dusts
and source sediments. Chemical Geology, 384: 16-26.

Jacobsen, S.B., Wasserburg, G.J., 1980. Sm-Nd isotopic evolution of chondrites Earth and Planetary Science Letters, 50(1): 139-155.

Jickells, T.D., An, Z.S., Andersen, K.K., Baker, A.R., Bergametti, G., Brooks, N., Cao, J.J., Boyd, P.W., Duce, R.A., Hunter, K.A., Kawahata, H., Kubilay, N., laRoche, J., Liss, P.S., Mahowald, N., Prospero, J.M., Ridgwell, A.J., Tegen, I., Torres, R., 2005. Global iron connections between desert dust, ocean biogeochemistry, and climate. Science, 308(5718): 67-71.

Johnson, A.H., Frizano, J., Vann, D.R., 2003. Biogeochemical implications of labile phosphorus in forest soils determined by the Hedley fractionation procedure. Oecologia, 135(4): 487-499.

Jolly, W.T., Lidiak, E., J., Dickin, A.P., Wu, T.-W., 1998. Geochemical diversity of Mesozoic island arc tectonic blacks in eastern Puerto Rico. In: Lidiak, E.G., Larue, D.K. (Eds.), Tectonics and Geochemistry of the Northeastern Caribbean. Geological Society of America Special Paper, Boulder, CO, pp. 67-98.

Kohfeld, K.E., Harrison, S.P., 2001. DIRTMAP: the geological record of dust. Earth-Science Reviews, 54(1-3): 81-114.

Kohl, C.P., Nishiizumi, K., 1992. Chemical isolation of quartz for measurement of in-situ produced cosmogenic nuclides. Geochimica Et Cosmochimica Acta, 56(9): 3583-3587.

Kumar, A., Abouchami, W., Galer, S.J.G., Garrison, V.H., Williams, E., Andreae, M.O., 2014. A radiogenic isotope tracer study of transatlantic dust transport from Africa to the Caribbean. Atmospheric Environment, 82: 130-143.

Kurtz, A.C., Derry, L.A., Chadwick, O.A., 2001. Accretion of Asian dust to Hawaiian soils: Isotopic, elemental, and mineral mass balances. Geochimica et Cosmochimica Acta, 65(12): 1971-1983.

Kurtz, A.C., Derry, L.A., Chadwick, O.A., Alfano, M.J., 2000. Refractory element mobility in volcanic soils. Geology, 28(8): 683-686.

Lal, D., 1991. Cosmic-ray labeling of erosion surfaces- in-sity nuclide production rates and erosion models. Earth and Planetary Science Letters, 104(2-4): 424-439.

Land, M., Ohlander, B., Ingri, J., Thunberg, J., 1999. Solid speciation and fractionation of rare earth elements in a spodosol profile from northern Sweden as revealed by sequential extraction. Chemical Geology, 160(1-2): 121-138.

Lawrence, C.R., Neff, J.C., 2009. The contemporary physical and chemical flux of aeolian dust: A synthesis of direct measurements of dust deposition. Chemical Geology, 267(1-2): 46-63.

Lawrence, D., D'Odorico, P., Diekmann, L., DeLonge, M., Das, R., Eaton, J., 2007. Ecological feedbacks following deforestation create the potential for a catastrophic ecosystem shift in tropical dry forest. Proceedings of the National Academy of Sciences of the United States of America, 104(52): 20696-20701.

Li, J.W., Zhang, G.L., Gong, Z.T., 2013. Nd isotope evidence for dust accretion to a soil chronosequence in Hainan Island. Catena, 101: 24-30.

Lindberg, S.E., Lovett, G.M., 1985. Field measurements of particle dry deposition rates to foliage and inert surfaces in a forest canopy. Environmental Science & Technology, 19(3): 238-244.

Liptzin, D., Silver, W.L., 2009. Effects of carbon additions on iron reduction and phosphorus availability in a humid tropical forest soil. Soil Biology & Biochemistry, 41(8): 1696-1702.

Longo, A.F., Ingall, E.D., Diaz, J.M., Oakes, M., King, L.E., Nenes, A., Mihalopoulos, N., Violaki, K., Avila, A., Benitez-Nelson, C.R., Brandes, J., McNulty, I., Vine, D.J., 2014. P-NEXFS analysis of aerosol phosphorus delivered to the Mediterranean Sea. Geophysical Research Letters, 41(11): 4043-4049.

Mage, S.M., Porder, S., 2013. Parent Material and Topography Determine Soil Phosphorus Status in the Luquillo Mountains of Puerto Rico. Ecosystems, 16(2): 284-294.

Mahowald, N., Jickells, T.D., Baker, A.R., Artaxo, P., Benitez-Nelson, C.R., Bergametti, G., Bond, T.C., Chen, Y., Cohen, D.D., Herut, B., Kubilay, N., Losno, R., Luo, C., Maenhaut, W., McGee, K.A., Okin, G.S., Siefert, R.L., Tsukuda, S., 2008. Global distribution of atmospheric phosphorus sources, concentrations and deposition rates, and anthropogenic impacts. Global Biogeochemical Cycles, 22(4).

Martin, J.H., 1990. Glacial-interglacial CO2 change: The iron hypothesis. Paleoceanography, 5(1): 1-13.

Masarik, J., Frank, M., Schafer, J.M., Wieler, R., 2001. Correction of in situ cosmogenic nuclide production rates for geomagnetic field intensity variations during the past 800,000 years. Geochimica Et Cosmochimica Acta, 65(17): 2995-3003.

McClintock, M.A., McDowell, W.H., Pett-Ridge, J.C., in press. Variability of African dust deposition in the Luquillo Mountains, Puerto Rico, based on rainfall chemistry and HYSPLIT airmass back-trajectory modeling. Journal of Geophysical Research-Atmospheres.

Meyer, V., Saatchi, S.S., Chave, J., Dalling, J.W., Bohlman, S., Fricker, G.A., Robinson, C., Neumann, M., Hubbell, S., 2013. Detecting tropical forest biomass dynamics from repeated airborne lidar measurements. Biogeosciences, 10(8): 5421-5438.

Moreno, T., Querol, X., Castillo, S., Alastuey, A., Cuevas, E., Herrmann, L., Mounkaila, M., Elvira, J., Gibbons, W., 2006. Geochemical variations in aeolian mineral particles from the Sahara-Sahel Dust Corridor. Chemosphere, 65(2): 261-270.

Muhs, D.R., Budahn, J.R., Prospero, J.M., Carey, S.N., 2007. Geochemical evidence for African dust inputs to soils of western Atlantic islands: Barbados, the Bahamas, and Florida. Journal of Geophysical Research-Atmospheres, 112: F02009.

Muhs, D.R., Crittenden, R.C., Rosholt, J.N., Bush, C.A., Stewart, K.C., 1987. Genesis of Marine Terrace Soils, Barbados, West-Indies - Evidence from Mineralogy and Geochemistry. Earth Surface Processes and Landforms, 12(6): 605-618.

Nakano, T., Yokoo, Y., Okumura, M., Jean, S.R., Satake, K., 2012. Evaluation of the Impacts of Marine Salts and Asian Dust on the Forested Yakushima Island Ecosystem, a World Natural Heritage Site in Japan. Water Air and Soil Pollution, 223(9): 5575-5597.

Nesbitt, H.W., Markovics, G., 1997. Weathering of granodioritic crust, long-term storage of elements in weathering profiles, and petrogenesis of siliciclastic sediments. Geochimica Et Cosmochimica Acta, 61(8): 1653-1670.

Nesbitt, H.W., Wilson, R.E., 1992. Recent chemical weathering og basalts. American Journal of Science, 292(10): 740-777.

Nishiizumi, K., Imamura, M., Caffee, M.W., Southon, J.R., Finkel, R.C., McAninch, J., 2007. Absolute calibration of Be-10 AMS standards. Nuclear Instruments & Methods in Physics Research Section B-Beam Interactions with Materials and Atoms, 258(2): 403-413.

Okin, G.S., Mahowald, N., Chadwick, O.A., Artaxo, P., 2004. Impact of desert dust on the biogeochemistry of phosphorus in terrestrial ecosystems. Global Biogeochemical Cycles, 18(2).

Pedersen, H.D., Postma, D., Jakobsen, R., Larsen, O., 2005. Fast transformation of iron oxyhydroxides by the catalytic action of aqueous Fe(II). Geochimica Et Cosmochimica Acta, 69(16): 3967-3977.

Pelletier, J.D., 2007. Cantor set model of eolian dust deposits on desert alluvial fan terraces. Geology, 35(5): 439-442.

Pelletier, J.D., Cook, J.P., 2005. Deposition of playa windblown dust over geologic time scales. Geology, 33(11): 909-912.

Pelt, E., Chabaux, F., Stille, P., Innocent, C., Ghaleb, B., Gerard, M., Guntzer, F., 2013. Atmospheric dust contribution to the budget of U-series nuclides in soils from the Mount Cameroon volcano. Chemical Geology, 341: 147-157.

Pett-Ridge, J.C., 2007. Mineral aerosol inputs, nutrient sources, and weathering processes in tropical soils of Puerto Rico and the Hawaiian Islands. Ph.D. Thesis, Cornell University, Ithaca, 218 pp.

Pett-Ridge, J.C., 2009. Contributions of dust to phosphorus cycling in tropical forests of the Luquillo Mountains, Puerto Rico. Biogeochemistry, 94(1): 63-80.

Pett-Ridge, J.C., Derry, L.A., Barrows, J.K., 2009a. Ca/Sr and Sr-87/Sr-86 ratios as tracers of Ca and Sr cycling in the Rio Icacos watershed, Luquillo Mountains, Puerto Rico. Chemical Geology, 267(1-2): 32-45.

Pett-Ridge, J.C., Derry, L.A., Kurtz, A.C., 2009b. Sr isotopes as a tracer of weathering processes and dust inputs in a tropical granitoid watershed, Luquillo Mountains, Puerto Rico. Geochimica et Cosmochimica Acta, 73: 25-43.

Plug, L.J., Gosse, J.C., McIntosh, J.J., Bigley, R., 2007. Attenuation of cosmic ray flux in temperate forest. Journal of Geophysical Research-Earth Surface, 112(F2).

Porder, S., Hilley, G.E., Chadwick, O.A., 2007. Chemical weathering, mass loss, and dust inputs across a climate by time matrix in the Hawaiian Islands Earth and Planetary Science Letters, 258: 414-427.

Porder, S., Paytan, A., Vitousek, P.M., 2005. Erosion and landscape development affect plant nutrient status in the Hawaiian Islands. Oecologia, 142(3): 440-449.

Porder, S., Ramachandran, S., 2013. The phosphorus concentration of common rocks-a potential driver of ecosystem P status. Plant and Soil, 367(1-2): 41-55.

Prospero, J.M., 1999. Long-term measurements of the transport of African mineral dust to the southeastern United States: Implications for regional air quality. Journal of Geophysical Research-Atmospheres, 104(D13): 15917-15927.

Prospero, J.M., Lamb, P.J., 2003. African droughts and dust transport to the Caribbean: Climate change implications. Science, 302(5647): 1024-1027.

Reheis, M.C., Goodmacher, J.C., Harden, J.W., McFadden, L.D., Rockwell, T.K., Shroba, R.R., Sowers, J.M., Taylor, E.M., 1995. Quaternary soils and dust deposition in southern Nevada and California Geological Society of America Bulletin, 107(9): 1003-1022.

Reid, E.A., Reid, J.S., Meier, M.M., Dunlap, M.R., Cliff, S.S., Broumas, A., Perry, K., Maring, H., 2003. Characterization of African dust transported to Puerto Rico by individual particle and size segregated bulk analysis. Journal of Geophysical Research-Atmospheres, 108(D19).

Riebe, C.S., Kirchner, J.W., Finkel, R.C., 2003. Long-term rates of chemical weathering and physical erosion from cosmogenic nuclides and geochemical mass balance. Geochimica et Cosmochimica Acta, 67(22): 4411-4427.

Schulz, M.S., White, A.F., 1999. Chemical weathering in a tropical watershed, Luquillo mountains, Puerto Rico III: Quartz dissolution rates. Geochimica Et Cosmochimica Acta, 63(3-4): 337-350.
Shafer, D.S., Young, M.H., Zitzer, S.F., Caldwell, T.G., McDonald, E.V., 2007. Impacts of interrelated biotic and abiotic processes during the past 125 000 years of landscape evolution in the Northern Mojave Desert, Nevada, USA. Journal of Arid Environments, 69(4): 633-657.
Shinn, E.A., Smith, G.W., Prospero, J.M., Betzer, P., Hayes, M.L., Garrison, V., Barber, R.T., 2000. African dust and the demise of Caribbean coral reefs. Geophysical Research Letters, 27(19): 3029-3032.
Silver, W.L., Scatena, F.N., Johnson, A.H., Siccama, T.G., Sanchez, M.J., 1994. Nutrient availability in a montane wet tropical forest : Spatial patterns and methodological considerations. Plant and Soil, 164(1): 129-145.
Singer, A., Dultz, S., Argaman, E., 2004. Properties of the non-soluble fractions of suspended dust over the Dead Sea. Atmospheric Environment, 38(12): 1745-1753.
Soderberg, K., Compton, J.S., 2007. Dust as a nutrient source for fynbos ecosystems, South Africa. Ecosystems, 10(4): 550-561.
Staiger, J., Gosse, J., Toracinta, R., Oglesby, B., Fastook, J., Johnson, J.V., 2007. Atmospheric scaling of cosmogenic nuclide production: Climate effect. Journal of Geophysical Research-Solid Earth, 112(B2).
Stallard, R.F., 2001. Possible environmental factors underlying amphibian decline in eastern Puerto Rico: Analysis of US government data archives. Conservation Biology, 15(4): 943-953.
Stoorvogel, J.J., VanBreemen, N., Janssen, B.H., 1997. The nutrient input by Harmattan dust to a forest ecosystem in Cote d'Ivoire, Africa. Biogeochemistry, 37(2): 145-157.
Swap, R., Garstang, M., Greco, S., Talbot, R., Kallberg, P., 1992. Saharan dust in the Amazon Basin. Tellus Series B-Chemical and Physical Meteorology, 44(2): 133-149.
Tegen, I., Lacis, A.A., Fung, I., 1996. The influence on climate forcing of mineral aerosols from disturbed soils. Nature, 380(6573): 419-422.
Tiessen, H., Moir, J.O., 1993. Characterization of available P by sequential extraction, Soil Sampling Methods of Analysis. Canadian Society of Soil Science, Boca Raton, pp. 75-86.
Tishchenko, V., Meile, C., Scherer, M.M., Pasakarnis, T.S., Thompson, A., 2015. Fe2+ catalyzed iron atom exchange and re-crystallization in a tropical soil. Geochimica et Cosmochimica Acta, 148: 191-202.
Trapp, J.M., Millero, F.J., Prospero, J.M., 2010. Temporal variability of the elemental composition of African dust measured in trade wind aerosols at Barbados and Miami. Marine Chemistry, 120(1-4): 71-82.
USDA, 2002. Soil Survey of Caribbean National Forest and Luquillo Experimental Forest, Commonwealth of Puerto Rico. In: USDA (Editor). Natural Resources Conservation Service, Washington, DC.
Viers, K., Wasserburg, G.J., 2004. Behavior of Sm and Nd in a lateritic soil profile. Geochimica Et Cosmochimica Acta, 68(9): 2043-2054.
Vitousek, P.M., Porder, S., Houlton, B.Z., Chadwick, O.A., 2010. Terrestrial phosphorus limitation: mechanisms, implications, and nitrogen-phosphorus interactions. Ecological Applications, 20(1): 5-15.
Walker, T.W., Syers, J.K., 1976. Fate of phosphorus during pedogenesis. Geoderma, 15(1): 1-19.
Walter, A.V., Nahon, D., Flicoteaux, R., Girard, J.P., Melfi, A., 1995. Behaviour of major and trace elements and fractionation of REE under tropical weathering of a typical apatite-rich carbonatite from Brazil. Earth and Planetary Science Letters, 136(3-4): 591-602.
White, A.F., Blum, A.E., Schulz, M.S., Vivit, D.V., Stonestrom, D.A., Larsen, M., Murphy, S.F., Eberl, D., 1998. Chemical weathering in a tropical watershed, Luquillo Mountains, Puerto Rico: I. Long-term versus short-term weathering fluxes. Geochimica et Cosmochimica Acta, 62(2): 209-226.
White, E.J., Turner, F., 1970. Method of estimating income of nutrients in a catch of airborne particles by a woodland canopy. Journal of Applied Ecology, 7(3): 441-461.
Yang, X., Post, W.M., 2011. Phosphorus transformations as a function of pedogenesis: A synthesis of soil phosphorus data using Hedley fractionation method. Biogeosciences, 8(10): 2907-2916.
Zarin, D.J., Johnson, A.H., 1995. Nutrient accumulation during primary succession in a montane tropical forest, Puerto Rico. Soil Science Society of America Journal, 59(5): 1444-1452.
Zhang, J., Shao, Y., Huang, N., 2014. Measurements of dust deposition velocity in a wind-tunnel experiment. Atmospheric Chemistry and Physics, 14(17): 8869-8882.

Figure Captions

Figure 1. Location of the ridgetop sampling sites within the Luquillo Mountains. Colors of sample location points indicate the % of Nd in 0-20 cm ridgetop soil that is African dust-derived based on εNd values.

Figure 2. Colors of sample location points indicate the soil dust content (%) based on the % dust-derived Nd (Figure 1) and the Nd content of both the soil and dust.

Figure 3. Two-component mixing diagram of $^{87}Sr/^{86}Sr$ vs εNd for Luquillo Mountains 0-20 cm depth ridgetop soils. The solid line shows a mixture between total atmospheric input and saprolite, dashed line shows a mixture between total atmospheric input and underlying bedrock, dashed and dotted line shows a mixture between African dust and underlying bedrock, and the dotted line shows a mixture of African dust and saprolite. Isotopic endmembers and Sr and Nd concentrations are given in Table 2 caption and in Pett-Ridge et al (2007; 2009a; 2009b). εNd of African dust and total atmospheric input are assumed identical given negligible Nd contribution from seawater. The saprolite elemental and isotopic composition is based on a mid-profile sample collected at 4 m depth in the 8 m deep LG1 soil and saprolite profile on quartz diorite bedrock (Pett-Ridge et al., 2009b).

Figure 4. Variation in soil % dust content based on underlying bedrock type. Boxes represent the 25th and 75th percentiles, horizontal lines within each box represent medians, and whiskers

indicate the 5th and 95th percentiles; symbols indicate outliers that fall more than 1.5x the inter-quartile range from the median.

Figure 5. ^{10}Be-based denudation rates for 16 ridgetop sites on quartz diorite bedrock in relation to variation in soil dust content. Error bars represent the full range of calculated denudation rates depending if low quartz enrichment of 27% or high quartz enrichment of 91% is used. See online annex for details.

Figure 6. Soil dust content in relation to ridge-width for quartz diorite-derived soils. Dashed line represents a linear regression with $r^2 = 0.66$, and $p=0.01$.

Figure 7. (a) The sum of HCO_3 + NaOH extractable P and (b) total P in relation to soil dust content, for quartz diorite-derived soils. Linear regression for total P vs. soil dust has $r^2 = 0.25$, $p=0.03$; linear regression for extractable P vs. soil dust has $r^2 = 0.24$, $p=0.04$.

Table 1. Site physiography for ridgetop soils

Sample	Longitude (degrees)	Latitude (degrees)	Elevation (m)	Ridge width (m)	Forest Type	Soil type	Bedrock Type	Annual Rainfall (mm)*
SM1	-65.8485	18.2773	797		Colorado	Oxisols	VC	4130
SM10	-65.8260	18.3100	521		Colorado	Oxisols	VC	3790
SM19	-65.8397	18.2656	740		Colorado	Oxisols	VC	4070
SM28	-65.8297	18.3204	441		Tabonuco	Oxisols	VC	3660
SM37	-65.7412	18.3156	376		Tabonuco	Oxisols	VC	3540
SM46	-65.8159	18.3183	582		Tabonuco	Oxisols	VC	3870
SM55	-65.8183	18.3099	616		Colorado	Oxisols	VC	3920
SM64	-65.8525	18.2743	694		Tabonuco	Oxisols	VC	4020
SM82	-65.7703	18.3042	444		Tabonuco	Oxisols	VC	3660
SM73	-65.7858	18.2961	778		Colorado	Inceptisols	QD	4110
SM91	-65.7956	18.2921	785		Colorado	Inceptisols	QD	4120
SM100	-65.7858	18.2714	661		Colorado	Inceptisols	QD	3980
SM109	-65.7944	18.2706	538		Colorado	Inceptisols	QD	3810
SM118	-65.8030	18.2636	584		Tabonuco	Inceptisols	QD	3880
SM127	-65.7959	18.2679	565		Tabonuco	Inceptisols	QD	3850
SM136	-65.7935	18.2631	379		Tabonuco	Inceptisols	QD	3540
PRCT-1	-65.7856	18.2710	678	17	Colorado	Inceptisols	QD	4000
PRCT-2	-65.7860	18.2719	685	5	Colorado	Inceptisols	QD	4010
PRCT-3	-65.7872	18.2721	674	9	Colorado	Inceptisols	QD	3990
PRCT-4	-65.7877	18.2747	687	11	Colorado	Inceptisols	QD	4010
PRCT-5	-65.7883	18.2724	697	14	Colorado	Inceptisols	QD	4020
PRCT-6	-65.7906	18.2810	710	11	Colorado	Inceptisols	QD	4040
PRCT-7	-65.7900	18.2900	683	21	Colorado	Inceptisols	QD	4000
PRCT-8	-65.7963	18.2919	760	26	Colorado	Inceptisols	QD	4100
PRCT-9	-65.7977	18.2927	772	54	Colorado	Inceptisols	QD	4110
PRCT-10	-65.7960	18.2894	815	42	Colorado	Inceptisols	QD	4150
PRCT-11	-65.7949	18.2905	795	15	Colorado	Inceptisols	QD	4130
PRCT-12	-65.7907	18.2884	668	21	Colorado	Inceptisols	QD	3990
PRGB140324-3	-65.7792	18.2667	551	2	Colorado	Inceptisols	QD	3830
PRGB140323-4	-65.8038	18.2740	699	2	Colorado	Inceptisols	QD	4020
PRGB140323-5	-65.8052	18.2721	657	2	Colorado	Inceptisols	QD	3970

* estimated rainfall based on PRISM model (Daly et al., 2003).

VC denotes volcaniclastic, QD denotes quartz diorite

The datum WGS84 was used for longitude and latitude coordinates.

Sample SM82 was originally classified as having a quartz diorite parent material, but further analysis revealed the parent material of that soil was volcaniclastic.

Table 2. Elemental and isotopic chemistry for ridgetop soils.

Sample	Nd	Fe_2O_3%	Nb	τNd (Nb)	ϵ_{Nd}	%dust Nd	1 s.d.	$^{87}Sr/^{86}Sr$	Soil dust	1 s.d.
	mg g^{-1}	wt %	mg g^{-1}				±		%	±
SM1 (VC)	4.30	10.6	7.45	-0.93	-8.1	81	7	0.70530	8.1	1.5
SM10 (VC)	0.77	10.8	6.17	-0.99	-10.3	92	8	0.71262	1.7	0.3
SM19 (VC)	1.76	10.6	7.31	-0.97	-7.2	77	7	0.71208	3.1	0.6
SM28 (VC)	3.12	12.6	5.96	-0.94	-5.1	66	6	0.71052	4.8	0.9
SM37 (VC)	4.16	11.2	5.66	-0.92	1.0	35	5	0.71002	3.4	0.7
SM46 (VC)	4.69	12.4	7.30	-0.93	0.9	35	5	0.70618	3.9	0.8
SM55 (VC)	4.92	12.7	7.95	-0.93	-0.8	44	5	0.71107	5.0	1.0
SM64 (VC)	3.03	9.8	5.64	-0.94	3.0	25	4	0.70982	1.7	0.4
SM82 (VC)	2.37	12.3	5.30	-0.95	-5.9	70	6	0.71417	3.9	0.7
SM73	3.13	3.2	4.18	-0.83	3.2	21	4	0.70418	1.5	0.4
SM91	1.22	3.3	2.94	-0.90	3.8	18	4	0.71068	0.5	0.1
SM100	2.16	6.1	3.91	-0.87	2.3	26	4	0.71062	1.3	0.3
SM109	0.51	3.4	2.70	-0.96	-6.2	70	6	0.71237	0.8	0.2
SM118	1.76	4.1	2.48	-0.84	5.5	9	4	0.71097	0.4	0.2
SM127	8.98	4.7	2.39	-0.14	5.9	7	4		1.5	0.8
SM136	3.66	5.6	2.72	-0.69	1.9	28	4	0.70558	2.4	0.5
PR-CT-1	0.66	4.2	4.47	-0.97	-2.7	52	5	0.71197	0.8	0.2
PR-CT-2	1.00	8.2	4.07	-0.89	-7.1	75	6	0.71352	1.8	0.3
PR-CT-3	0.20	7.6	5.44	-0.99	-2.6	52	5	0.71152	0.2	0.0
PR-CT-4	0.86	4.9	4.58	-0.96	-4.8	63	6	0.71333	1.3	0.2
PR-CT-5	0.80	4.9	3.94	-0.93	-5.5	67	6	0.71420	1.2	0.2
PR-CT-6	2.23	4.7	4.04	-0.87	3.0	22	4	0.71247	1.1	0.3
PR-CT-7	1.90	4.2	3.53	-0.80	1.6	29	4	0.70964	1.3	0.3
PR-CT-8	2.07	2.3	5.44	-0.91	-3.3	55	5	0.71018	2.7	0.5
PR-CT-9	2.53	2.3	7.67	-0.92	-5.9	69	6	0.71444	4.1	0.8
PR-CT-10	1.77	2.5	8.41	-0.95	-4.1	59	6	0.71196	2.4	0.5
PR-CT-11	1.00	3.4	4.13	-0.88	-0.7	41	5	0.71167	1.0	0.2
PR-CT-12	0.40	5.6	4.10	-0.95	-6.4	72	6	0.71534	0.7	0.1
PRGB140324-3	7.61		4.37	-0.60	7.3	-1	-4		-0.1	0.6
PRGB140323-4	0.78		5.08	-0.96	-8.5	82	7		1.5	0.3
PRGB140323-5	1.98		2.92	-0.84	6.5	3	4		0.2	0.2
Dust	43		12.00	-	-11.8			0.71788		
Quartz diorite	7.95		1.83	-	7.2			0.70409		
Volcaniclastic	12.91		1.47	-	7.8			0.70358		

Quart Diorite bedrock Nb value is average of 31 samples (s.d.=0.24). Nd is average of 15 samples (s.d.=1.05)

Volcaniclastic bedrock Nb value is average of 55 samples (s.d.= 0.55). Nd is average of 28 samples (s.d.=4.85)

ϵNd of dust, -11.8, is average of Caribbean aerosols reported in Kumar et al (2014) and Grousset et al (1988), (n=16, 1 s.d. = 1.2). ϵNd of volcaniclastic bedrock is the average of 5 reported values for the Martin Gonzalez, Lomas, and Fajardo formations (range of 7.09 to 8.55 ϵNd, s.d.= 0.69) (Jolly et al 1998, Frost et al 1998); ϵNd of quartz diorite is average of 7 values for the Rio Blanco stock (of which 2 are newly analyzed and 5 are previously published (Chabaux et al 2013, Pett-Ridge et al 2009, Frost et al 1998).

[Nd] of dust is based on Carribeean aerosols reported in Grousset et al (1988 and 1992), Muhs et al (1987), and Trapp et al (2010) (1 s.d. = 6.9 ppm, n=44).

$^{87}Sr/^{86}Sr$ dust and bedrock is from Pett-Ridge et al (2009) and Smith et al (1998), [Sr] of Saharan dust is 294 ppm, [Sr] of quartz diorite is 211 ppm, +/- 23, and [Sr] of volcaniclastic is 534 ppm, +/- 276.

Table 3. Denudation rates for quartz diorite-derived ridgetop soils

Sample	Denudation rate* (mm ka^{-1})	Mean residence time for top 20 cm soil (ka)
SM73	53 ± 11	1.9
SM91	60 ± 12	1.7
SM100	43 ± 9	2.3
SM109	73 ± 3	1.4
SM118	63 ± 2	1.6
SM127	69 ± 2	1.5
PR-CT-1	42 ± 9	2.4
PR-CT-2	56 ± 11	1.8
PR-CT-4	44 ± 9	2.3
PR-CT-5	46 ± 9	2.2
PR-CT-6	53 ± 11	1.9
PR-CT-8	57 ± 12	1.7
PR-CT-9	46 ± 9	2.2
PR-CT-10	71 ± 14	1.4
PR-CT-11	60 ± 12	1.7
PR-CT-12	55 ± 11	1.8

*Mean of low and high quartz enrichment is shown, ± indicates the full range of calculated denudation rates depending if low quartz enrichment of 27% or high quartz enrichment of 91% is used. See online annex for details.

Table 4. Soil phosphorus and carbon chemistry

Sample	NaHCO3-Pi	NaHCO3-Po	NaHCO3-Pt	NaOH-Pi	NaOH-Po	NaOH-Pt	Residual P	Total P	Carbon
	mg g^{-1}	mg g^{-1}	mg g^{-1}	mg g^{-1}	mg g^{-1}	mg g^{-1}	mg g^{-1}	mg g^{-1}	%
SM1	0.2	7.2	7.4	19	54	73	132	213	6.2
SM10	0.2	4.2	4.3	44	19	63	122	193	5.2
SM19	0.0	8.4	8.4	27	113	141	58	209	7.0
SM28	0.4	5.4	5.8	45	50	95	98	202	4.7
SM37	0.0	3.1	3.1	20	54	74	131	210	2.8
SM46	1.6	5.8	7.4	26	52	78	220	307	3.6
SM55	0.3	4.0	4.4	22	54	76	82	163	6.9
SM64	0.0	9.9	9.9	31	81	111	115	236	6.2
SM82	1.1	9.0	10.1	52	33	85	139	237	5.7
SM73	0.0	5.1	5.1	8	63	71	16	93	5.4
SM91	0.1	5.4	5.5	11	63	74	13	94	4.4
SM100	1.9	6.9	8.9	50	37	88	53	154	2.6
SM109	1.6	3.8	5.4	12	50	62	14	82	2.7
SM118	0.9	4.7	5.6	14	56	69	75	153	2.6
SM127	0.2	6.5	6.6	13	76	89	52	149	2.7
SM136	4.5	5.4	9.9	19	111	130	75	217	1.7
PR-CT-1	0.8	2.4	3.2	13	35	49	123	175	4.3
PR-CT-2	0.5	2.8	3.4	20	38	59	134	196	4.8
PR-CT-3	0.9	2.4	3.3	21	40	61	158	223	5.2
PR-CT-4	1.4	2.5	3.9	19	41	61	132	196	4.8
PR-CT-5	0.9	2.4	3.3	13	33	47	107	157	5.6
PR-CT-6	0.0	3.1	3.1	10	23	33	117	153	3.8
PR-CT-7	1.1	2.1	3.2	14	32	46	99	148	6.0
PR-CT-8	3.1	1.7	4.7	30	44	75	117	196	14.0
PR-CT-9	3.7	3.4	7.1	30	49	79	124	210	13.5
PR-CT-10	5.4	2.0	7.4	42	74	116	151	275	16.6
PR-CT-11	0.4	1.7	2.1	12	26	38	99	140	4.1
PR-CT-12	0.4	2.3	2.7	13	33	46	100	148	5.1

Phosphorus data for the SM samples was previously analyzed as part of a larger dataset in Mage and Porder (2013).

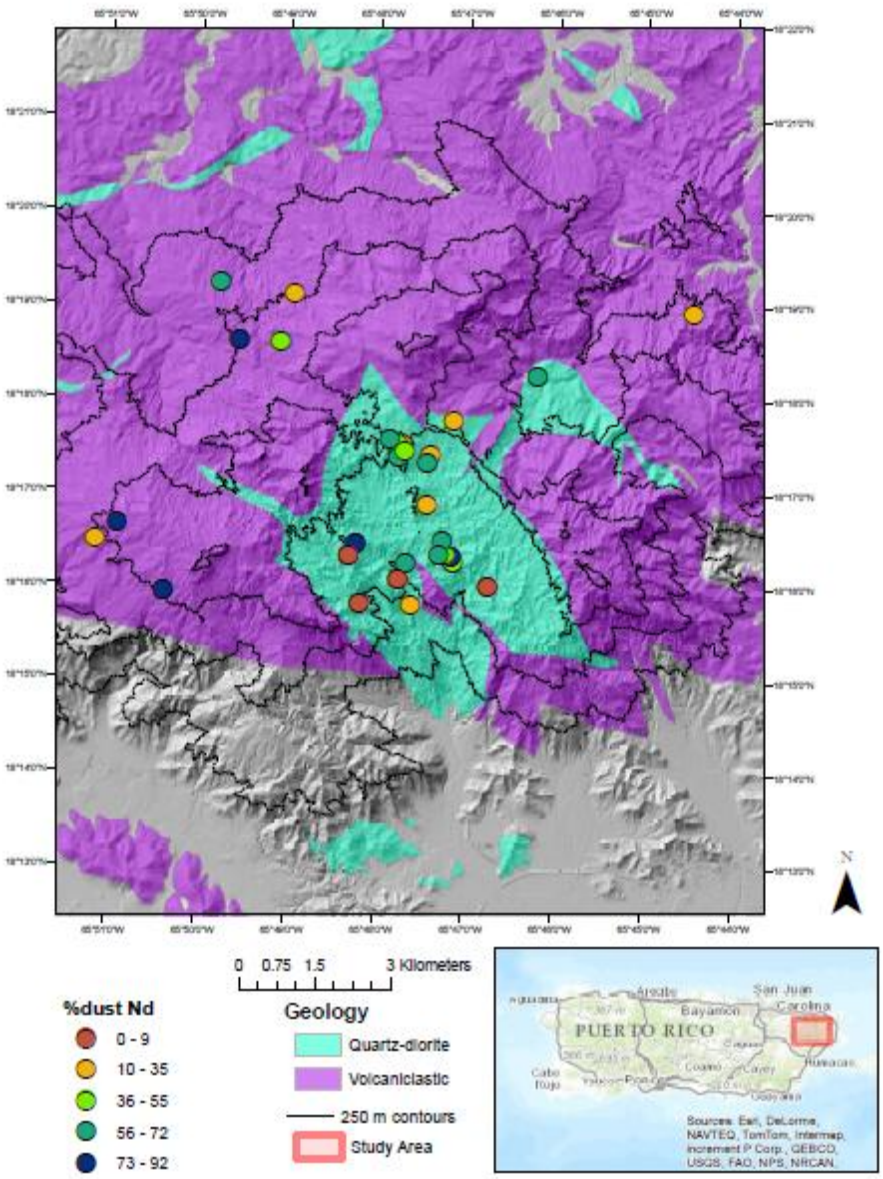

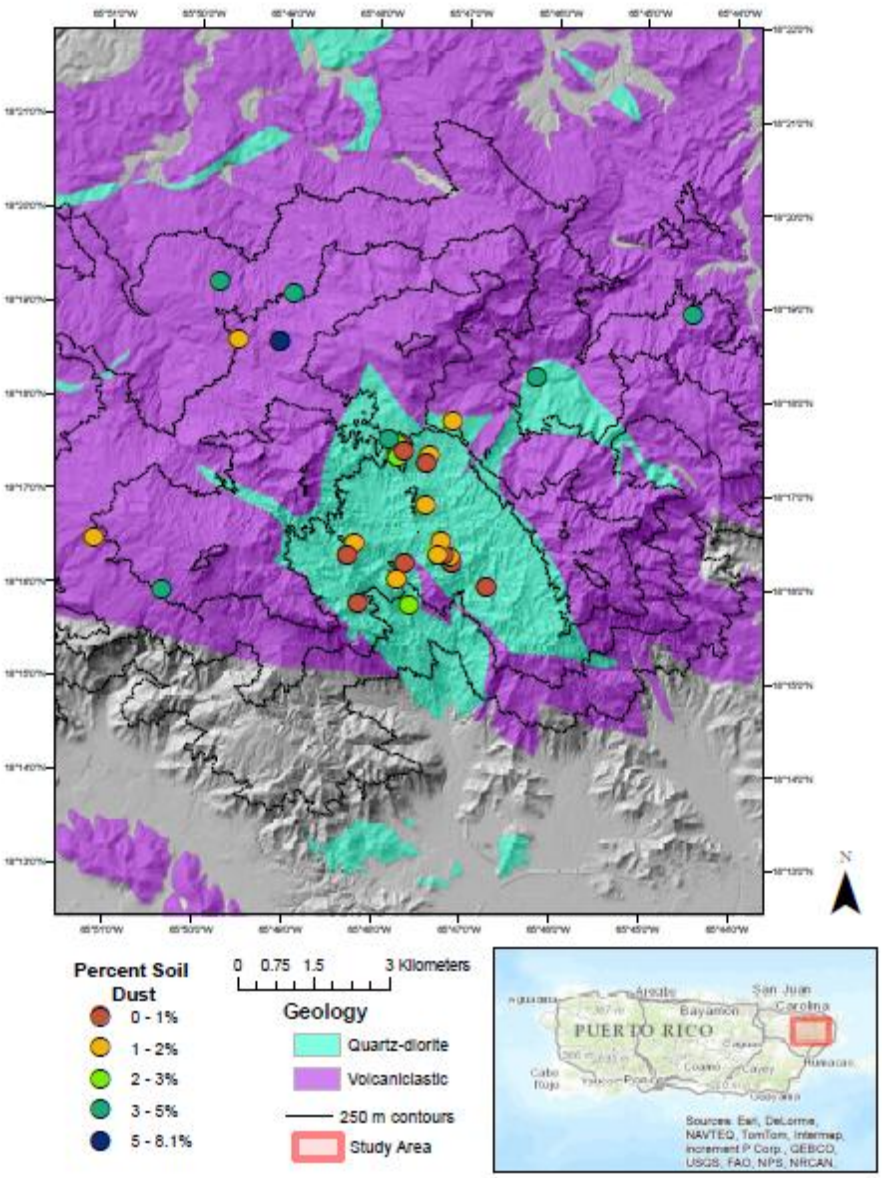

Figure 2

Figure 3

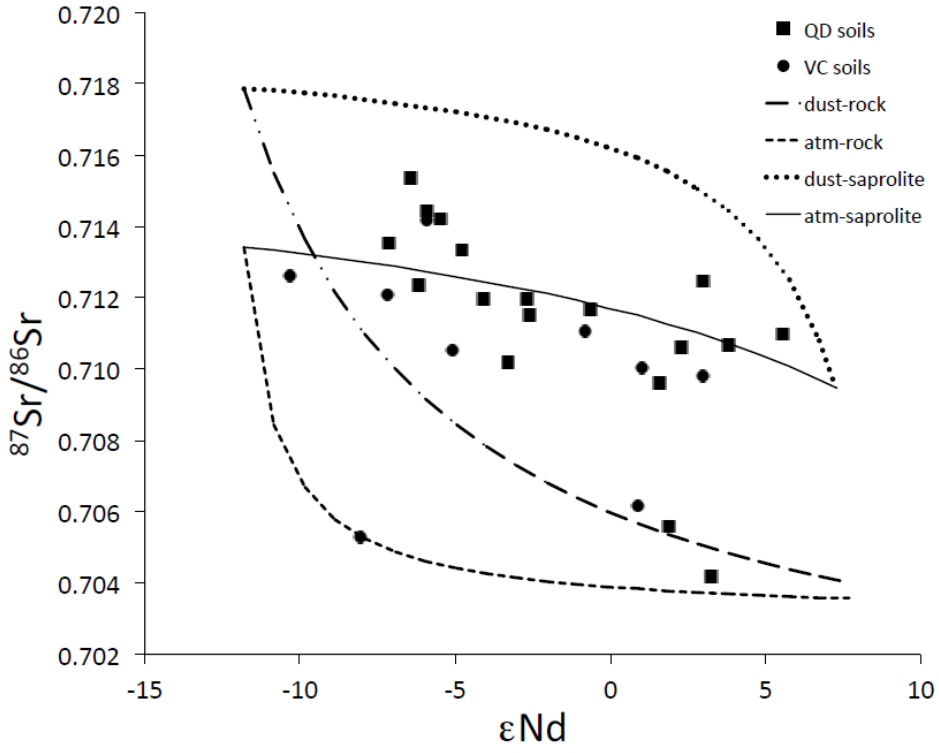

Figure 4

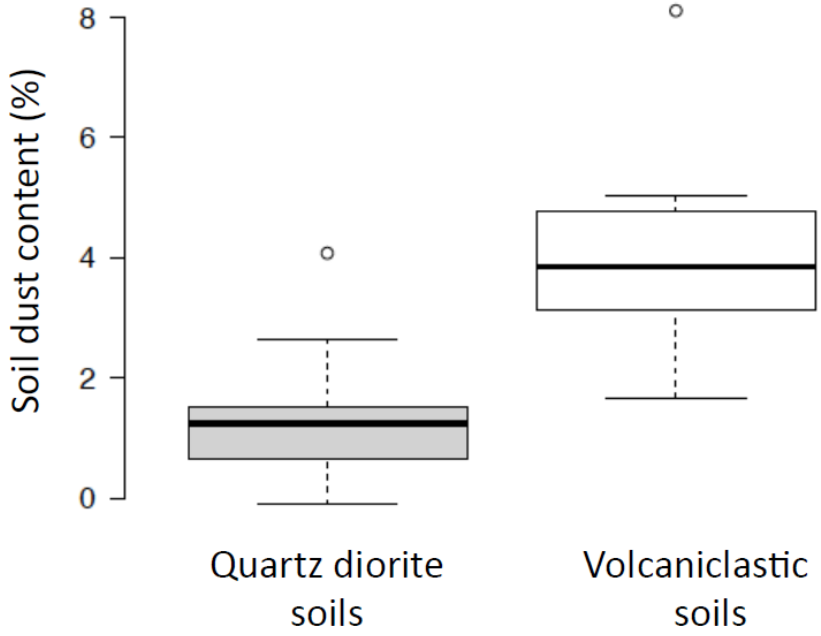

Figure 5

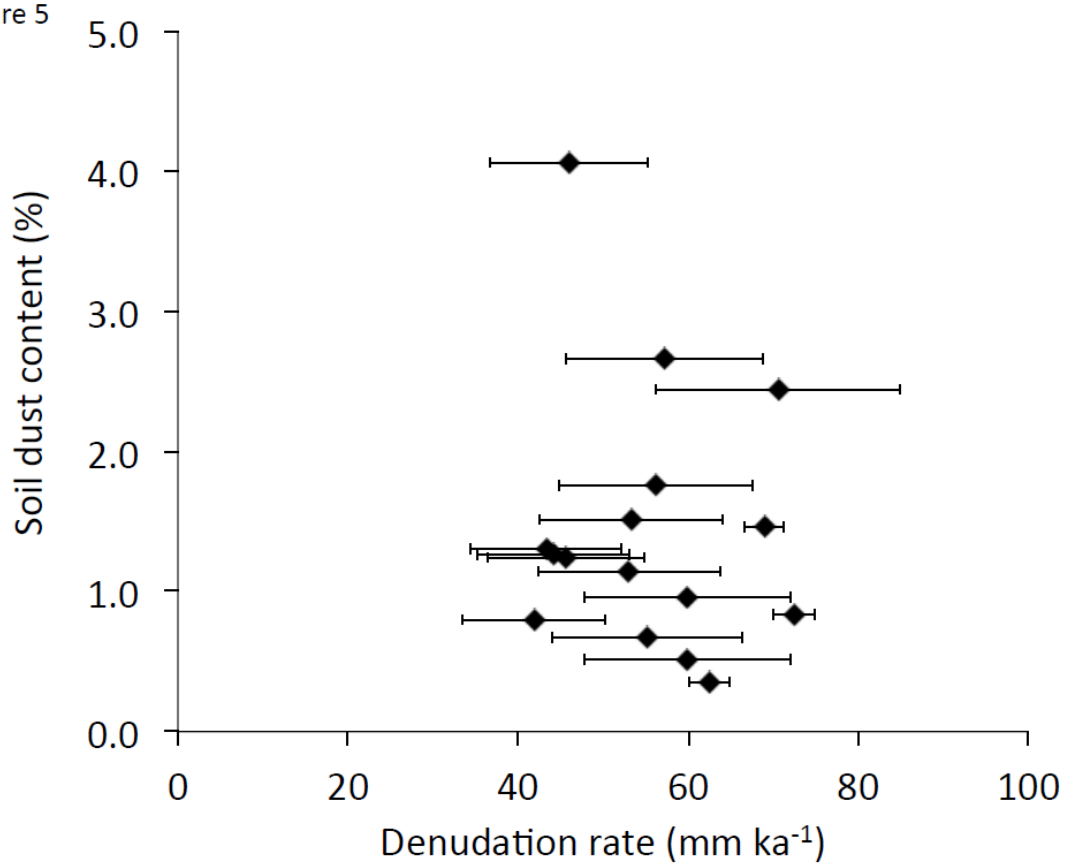

Figure 6

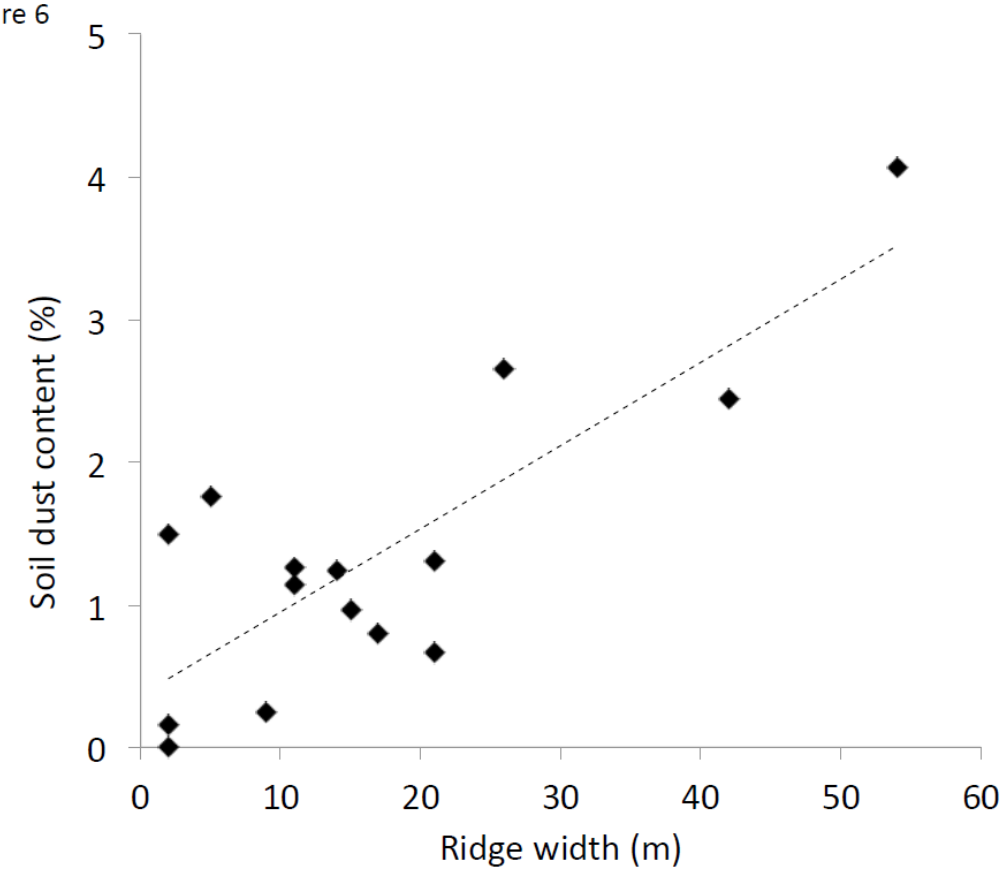

Figure 7